

**Reversible Fe(II) Uptake/Release by Magnetite Nanoparticles**

Journal:	<i>Environmental Science: Nano</i>
Manuscript ID	EN-ART-03-2018-000328.R3
Article Type:	Paper
Date Submitted by the Author:	01-Jun-2018
Complete List of Authors:	Peng, Huan; China University of Geosciences Pearce, Carolyn; Pacific Northwest National Laboratory Huang, Weifeng; Peking University Zhu, Zhenli; China University of Geosciences N'Diaye, Alpha T. ; Lawrence Berkeley National Laboratory Rosso, Kevin; Pacific Northwest National Laboratory, Liu, Juan; Peking University, College of Environmental Sciences and Engineering

## Environmental significance

The coexistence of magnetite and  $\text{Fe}^{2+}_{(\text{aq})}$  is common in anoxic subsurface environments and can have a great influence on important biogeochemical redox processes. This study demonstrates that the flow direction of electron equivalents that in the form of Fe(II) across the magnetite-solution interface changes in a predictable fashion by altering solution pH, background  $\text{Fe}^{2+}_{(\text{aq})}$  concentration, and magnetite loading. The equilibrium distribution of Fe(II) in the magnetite-solution system, across a range of conditions relevant to natural aquatic environments, can significantly change the stoichiometry and reactivity of magnetite nanoparticles, and also may influence redox-cycling, contaminant transformation, and microbial extracellular respiration in surrounding environments.

## Reversible Fe(II) Uptake/Release by Magnetite Nanoparticles

Huan Peng<sup>1,2</sup>, Carolyn I. Pearce<sup>3</sup>, Weifeng Huang<sup>4</sup>, Zhenli Zhu<sup>2,\*</sup>, Alpha T. N'Diaye<sup>5</sup>,  
Kevin M. Rosso<sup>3</sup>, Juan Liu<sup>1,6,\*</sup>

<sup>1</sup>The Key Laboratory of Water and Sediment Sciences, Ministry of Education, College of Environmental Sciences and Engineering, Peking University, Beijing 100871, China

<sup>2</sup>State Key Laboratory of Biogeology and Environmental Geology, School of Earth Sciences, China University of Geosciences, Wuhan, Hubei 430074, China

<sup>3</sup>Pacific Northwest National Laboratory, Richland, WA 99352, USA

<sup>4</sup>College of Engineering, Peking University, Beijing 100871, China

<sup>5</sup>Advanced Light Source, Lawrence Berkeley National Laboratory, Berkeley, CA 94720, USA

<sup>6</sup>Beijing Key Laboratory of Mineral Environmental Function, Peking University, Beijing 100871, China

To be submitted to *Environmental Science: Nano*

\* Corresponding authors:

J. L.

Address: College of Environmental Sciences and Engineering, Peking University, Beijing 100871, China

Email: [juan.liu@pku.edu.cn](mailto:juan.liu@pku.edu.cn)

Z. Z.

Address: State Key Laboratory of Biogeology and Environmental Geology, School of Earth Sciences, China University of Geosciences, Wuhan, Hubei 430074, China

Email: [zlzhu@cug.edu.cn](mailto:zlzhu@cug.edu.cn)

23 **ABSTRACT:**

24 Magnetite commonly coexists with aqueous  $\text{Fe}^{2+}$  ( $\text{Fe}^{2+}_{(\text{aq})}$ ) in anoxic subsurface environments.

25 Complex interactions between magnetite and  $\text{Fe}^{2+}_{(\text{aq})}$  profoundly impact redox potential

26 fluctuations in surrounding environment and biogeochemical cycles of important elements and

27 contaminants. However, the ability of magnetite to act as a source/sink of electron equivalents

28 through fluctuations in solution pH or the activity of  $\text{Fe}^{2+}_{(\text{aq})}$  remains poorly quantified. We

29 systematically studied the interrelationships between equilibrium  $\text{Fe}^{2+}_{(\text{aq})}$  concentrations and

30 structural versus surface-localized Fe(II)/Fe(III) ratios in magnetite using micro X-ray diffraction

31 and synchrotron-based X-ray magnetic circular dichroism, respectively, under different controlled

32 experimental conditions. Relative to pH 7, at pH 6 proton-promoted dissolution yields  $\text{Fe}^{2+}_{(\text{aq})}$

33 release from magnetite nanoparticles, coupled to a decrease in the structural Fe(II)/Fe(III) ratio by

34 electron hopping along the octahedral sublattice from the particle interior to the surface. At pH 8,

35 magnetite sorbs  $\text{Fe}^{2+}_{(\text{aq})}$ , increasing both the structural and surface-localized Fe(II)/Fe(III) ratio.

36 Amendments of  $\text{Fe}^{2+}_{(\text{aq})}$  inhibit acidic  $\text{Fe}^{2+}_{(\text{aq})}$  release and promote  $\text{Fe}^{2+}_{(\text{aq})}$  uptake at more basic

37 conditions, whereas increasing magnetite loading facilitates  $\text{Fe}^{2+}_{(\text{aq})}$ -magnetite interaction at the

38 same respective pH extremes. The reversible flow of Fe(II) across the magnetite-solution interface

39 under different conditions implies that the redox reactivity of magnetite nanoparticles is quickly

40 responsive to changes in environmental conditions, such as an increase in pH due to groundwater

41 passing through carbonate-rich rocks, via a dynamic redistribution of electron equivalents between

42 particle interiors and the solid/water interface.

## 1. Introduction

In anoxic aquifers, magnetite is one of the most common Fe(II)-containing minerals, playing an important role in a variety of biogeochemical processes, including immobilization of heavy metals and radioactive elements,<sup>1, 2</sup> degradation or sorption of organic/inorganic contaminants,<sup>3</sup> and supplying electrons for microbial respiration.<sup>4</sup> Naturally occurring magnetite nanoparticles (NPs) can be generated via various biotic or abiotic processes.<sup>5-7</sup> In addition, increasing interests in the use of magnetite NPs for environmental treatments,<sup>8</sup> biomedical applications,<sup>9</sup> and many other industrial implications, may lead to the unintentional release of engineered magnetite NPs into the environment. Therefore, it is important to develop a more comprehensive understanding of the transformation and reactivity of magnetite NPs in complex environmental systems.

The coexistence of magnetite and aqueous  $\text{Fe}^{2+}$  ( $\text{Fe}^{2+}_{(\text{aq})}$ ) is quite common in anoxic aquifers,<sup>3, 10</sup> as a result of various biogeochemical processes, such as the weathering of Fe(II)-bearing minerals, abiotic reduction of Fe(III) (oxyhydr)oxides, and dissimilatory iron reduction.<sup>11-13</sup> Previous studies have suggested that the presence of  $\text{Fe}^{2+}_{(\text{aq})}$  may significantly influence the stoichiometry, reactivity, and recrystallization of magnetite NPs in aqueous environment.<sup>3, 14-16</sup> The reaction of  $\text{Fe}^{2+}_{(\text{aq})}$  with magnetite NPs is of especially great interest in the field of environmental remediation, because the presence of magnetite NPs can distinctly enhance the reactivity of  $\text{Fe}^{2+}_{(\text{aq})}$  toward contaminant reduction.<sup>3, 14, 17, 18</sup> Also,  $\text{Fe}^{2+}_{(\text{aq})}$  may react with magnetite surface and change mobility or redox state of heavy metals.<sup>19, 20</sup> Despite its importance, molecular mechanisms of the interaction between  $\text{Fe}^{2+}_{(\text{aq})}$  and magnetite NPs have not been developed, in part due to the complexity of the magnetite/solution interface.<sup>19</sup>

To date, previous studies of the heterogeneous reactions between  $\text{Fe}^{2+}_{(\text{aq})}$  and iron oxides

1  
2  
3  
4 65 mainly focused on Fe(III)-(oxyhydr)oxides, such as goethite and hematite.<sup>21-25</sup> However,  
5  
6 66 magnetite, as a mixed-valent iron oxide, can be expected to react with  $\text{Fe}^{2+}_{(\text{aq})}$  differently from  
7  
8 67 Fe(III)-(oxyhydr)oxides, given its high electron mobility and facile topotactic interconversion with  
9  
10  
11 68 oxidized end-member maghemite.<sup>1,2,26</sup> Previous work focused on sorption isotherms and surface  
12  
13 69 complexation models of  $\text{Fe}^{2+}_{(\text{aq})}$  on magnetite, as well as the reduction of contaminants by ferrous  
14  
15 70 ions “sorbed on the magnetite surface”.<sup>27</sup> However, recent experimental findings revealed that, in  
16  
17  
18 71 low temperature (<100 °C) aqueous systems, interfacial electron transfer occurs between sorbed  
19  
20  
21 72 Fe(II) and lattice Fe(III) in the underlying magnetite, followed by bulk electron conduction and the  
22  
23 73 release of ferrous ions from other surface sites, i.e., atom exchange.<sup>27</sup> In addition, Gorski et al.  
24  
25 74 (2009) reported that the uptake of  $\text{Fe}^{2+}_{(\text{aq})}$  by partially oxidized magnetite at pH 7.2 increased the  
26  
27  
28 75 Fe(II)/Fe(III) ratio in the bulk magnetite structure and the corresponding reactivity of magnetite  
29  
30  
31 76 NPs.<sup>3</sup> However, the previous studies in this regard only examined a very limited range of  
32  
33 77 conditions, such as a fixed magnetite loading at pH 7.2.<sup>3, 14</sup> The extent of  $\text{Fe}^{2+}_{(\text{aq})}$ -magnetite  
34  
35 78 interaction and magnetite reactivity can be expected to vary substantially in response to fluctuating  
36  
37  
38 79 environmental conditions. For example, we have demonstrated in our previous work that the  
39  
40  
41 80 extent of Fe(II) release from (titano)magnetite decreases with increasing pH (pH = 6 - 8) but  
42  
43 81 increases with the content of Ti substitution at a fixed pH.<sup>1,4,26</sup> Thus, to completely understand the  
44  
45 82 role of magnetite NPs in natural environment, further studies are needed to systematically examine  
46  
47  
48 83 the correlation between the Fe(II)/Fe(III) ratio in magnetite structure and environmental variables.

49  
50 84 Here we investigate the effects of solution pH,  $\text{Fe}^{2+}_{(\text{aq})}$  amendment, and magnetite loading on  
51  
52  
53 85 the Fe(II)/Fe(III) ratio, which together control the redox reactivity of magnetite NPs. In particular,  
54  
55 86 we take advantage of sophisticated methods that we established in prior work to quantify the  
56  
57  
58  
59  
60

1  
2  
3  
4 87 Fe(II)/Fe(III) ratio in particle interiors versus that in the outermost few Ångstroms of particle  
5  
6 88 surfaces.<sup>1,26</sup> Micro X-ray Diffraction ( $\mu$ XRD) was performed on anoxic NP aqueous suspensions  
7  
8 89 before and after reactions with  $\text{Fe}^{2+}_{(\text{aq})}$  to infer the structural Fe(II)/Fe(III) ratio on the basis of the  
9  
10 90 measured cell parameter. Synchrotron-based Fe L-edge X-ray absorption (XA) and magnetic  
11  
12 91 circular dichroism (XMCD) spectroscopies were used to probe the Fe(II)/Fe(III) ratio at the  
13  
14 92 surface and to distinguish tetrahedral and octahedral Fe(II) and Fe(III).<sup>28</sup> Corresponding  
15  
16 93 equilibrium concentrations of  $\text{Fe}^{2+}_{(\text{aq})}$  in NP suspensions under various experimental conditions  
17  
18 94 were measured using wet chemical analysis. Through systematic study of the relationship between  
19  
20 95  $\text{Fe}^{2+}_{(\text{aq})}$  concentration in solution and structural Fe(II)/Fe(III) in the bulk and at surfaces, reversible  
21  
22 96 uptake and release of  $\text{Fe}^{2+}_{(\text{aq})}$  to and from sites in the magnetite structure was assessed as a  
23  
24 97 function of solution pH,  $\text{Fe}^{2+}_{(\text{aq})}$  amendment, and magnetite loading. The findings provided  
25  
26 98 insights into the equilibrium distribution of electron equivalents in the form of Fe(II) in the  
27  
28 99 magnetite-solution system, across a range of conditions relevant to natural aquatic environments.  
29  
30  
31  
32  
33  
34  
35  
36  
37  
38  
39

100

## 101 **2. Materials and Methods**

### 102 **2.1. Magnetite Synthesis and Characterization.**

103 Details about the chemical reagents and the anoxic glovebox used in this study are described  
104 in the Supporting Information (Section S1). Magnetite NPs were synthesized by a method  
105 modified from Pearce et al 2012,<sup>26</sup> via co-precipitating a stoichiometric mixture of 0.1 M  
106  $\text{FeCl}_2 \cdot 4\text{H}_2\text{O}$  and 0.2 M  $\text{FeCl}_3 \cdot 6\text{H}_2\text{O}$  ( $\text{Fe}^{2+}:\text{Fe}^{3+}$  mole ratio was 1:2) in the presence of ammonium  
107 ( $\text{NH}_4\text{OH}$ ) solution in the glovebox. With continuous stirring, a  $\text{N}_2$ -sparged ammonium solution  
108 (28% w/v) was added dropwise to the chloride solution at  $\sim 60$  °C, until precipitation was

1  
2  
3  
4 109 complete (pH = 9-11). After that, the suspension was continuously stirred for another 30 min.  
5  
6 110 Finally, the NPs were magnetically separated from the suspension and then washed three times  
7  
8 111 with degassed and deionized water (DDW) to remove excess iron salts. After the washing process,  
9  
10 112 the NPs were re-suspended in DDW and stored inside the glovebox in dark. More details about the  
11  
12 113 characterization of magnetite stoichiometry, NP concentration in the stock suspension, crystalline  
13  
14 114 phase, particle size and morphology, as well as specific surface area (SSA) are described in  
15  
16 115 Section S1.  
17  
18  
19  
20  
21  
22

## 23 117 **2.2. Heterogeneous Reactions between $\text{Fe}^{2+}_{(\text{aq})}$ and Magnetite NPs.**

24  
25 118 Concentration changes of dissolved ferrous ions ( $[\text{Fe}^{2+}_{(\text{aq})}]$ ) in the suspensions of 69 - 695 mg  
26  
27 119  $\text{L}^{-1}$  magnetite NPs (the equivalent Fe(II) concentration of 300 - 3000  $\mu\text{M}$ ) buffered at pH 6 - 8  
28  
29 120 with 0 - 1000  $\mu\text{M}$  added  $\text{Fe}^{2+}_{(\text{aq})}$  over time were measured. The buffer solution at pH 6 was 30 mM  
30  
31 121 MES solution, and that at pH 7 and 8 was 30 mM HEPES solution. Speciation distribution of 250  
32  
33 122 - 1000  $\mu\text{M}$   $\text{Fe}^{2+}_{(\text{aq})}$  in the buffer solution at pH 6 - 8 was calculated by Visual MINTEQ (Version  
34  
35 123 3.1, Jon Petter Gustafsson, KHT, Div. of Land and Water Resources Engineering, Stockholm,  
36  
37 124 Sweden). The results indicate that there is no significant difference in the speciation distribution of  
38  
39 125  $\text{Fe}^{2+}_{(\text{aq})}$  over the concentration range (0 - 1000  $\mu\text{M}$ ) studied (Table S1). The reaction between  
40  
41 126  $\text{Fe}^{2+}_{(\text{aq})}$  and magnetite NPs was initiated by spiking a given volume of magnetite stock suspension  
42  
43 127 to a buffer solution at the required pH and in presence of  $\text{FeSO}_4$  with a desired concentration in 10  
44  
45 128 mL sealed bottles. The reactors were continuously shaken using a rotating overhead shaker at a  
46  
47 129 speed of 10 rpm during reactions. Sample aliquots were taken over time and filtered using 0.22  
48  
49 130  $\mu\text{m}$  syringe filters.  $[\text{Fe}^{2+}_{(\text{aq})}]$  in the filtrates were determined by adding 0.2 mL of the filtrate to 1.8  
50  
51  
52  
53  
54  
55  
56  
57  
58  
59  
60



1  
2  
3  
4 131 mL ferrozine reagent (1 g L<sup>-1</sup> ferrozine in 30 mM HEPES buffer, pH 7.0) and then measuring the  
5  
6 132 absorbance at 562 nm by using a UV–visible spectrophotometer (Shimadzu UV-2501PC). All  
7  
8 133 experiments were carried out at least in triplicates. The activity coefficient of Fe<sup>2+</sup><sub>(aq)</sub> in the pH 7.0  
9  
10 134 buffer solution for thermodynamic calculation was 0.6, which was calculated using Extended  
11  
12 135 Debye–Huckel model (Visual Minteq software, v3.0).  
13  
14  
15  
16  
17

### 18 137 **2.3. Micro X-ray Diffraction (μXRD).**

19  
20 138 Crystalline phase and cell parameters of synthetic NPs before and after reaction with added  
21  
22 139 Fe<sup>2+</sup><sub>(aq)</sub> were determined by μXRD using a Rigaku D/Max Rapid II instrument with a MicroMax  
23  
24 140 007HF generator fitted with a rotating Cr anode ( $\lambda = 2.2897 \text{ \AA}$ ) and a 2D image plate detector.  
25  
26 141 The XRD patterns were analyzed using JADE 9.0 from Materials Data Inc., and the PDF4+  
27  
28 142 database from ICSD. Samples for μXRD measurements were prepared by loading the  
29  
30 143 concentrated NP suspensions into boron-rich 0.5 mm O.D. capillary tubes (Charles Supper  
31  
32 144 Company) in the glovebox, and then sealing the capillaries with capillary wax (Charles Supper  
33  
34 145 Company) to keep samples under anoxic conditions and in aqueous suspensions during  
35  
36 146 measurements. The cell parameter of magnetite was obtained by fitting all strong diffraction peaks  
37  
38 147 in XRD patterns using the pseudo-Voigt profile shape function. Based on the linear relationship  
39  
40 148 between cell parameter and structural Fe(II)/Fe(III) ratio in magnetite,<sup>26</sup> the change of structural  
41  
42 149 Fe(II)/Fe(III) ratio in magnetite NPs after reaction with Fe<sup>2+</sup><sub>(aq)</sub> was determined from the unit cell  
43  
44 150 parameters measured using μXRD. The details of data processing and determination of cell  
45  
46 151 parameters and structural Fe(II)/Fe(III) ratios were described previously.<sup>26</sup>  
47  
48  
49  
50  
51  
52  
53  
54  
55  
56  
57  
58  
59  
60

#### 153 **2.4. X-ray Magnetic Circular Dichroism (XMCD).**

154 To compare oxidation state and local structure of magnetically ordered iron cations at surface  
155 of magnetite NPs before and after the reactions with  $\text{Fe}^{2+}_{(\text{aq})}$ , synchrotron XMCD spectra of  
156 magnetite NPs were collected at room temperature on beamline 6.3.1 at the Advanced Light  
157 Source (ALS), Berkeley, CA. Samples were prepared by drying aliquots of the NP suspensions  
158 onto carbon tape attached to the sample manipulator in an anoxic cabinet, which were maintained  
159 under anoxic conditions until immediately prior to XMCD measurements. X-ray absorption (XA)  
160 spectra at the Fe  $L_{2,3}$  edges was collected in total-electron yield (TEY) mode with an effective  
161 probing depth of  $\sim 4.5$  nm.<sup>29</sup> At each energy point, XA spectra were measured for two opposite  
162 magnetization directions by reversing the applied field of 0.4 T. The XMCD spectrum was  
163 obtained as the difference between these two XA spectra after normalization to the incident beam  
164 intensity.<sup>30</sup> The ratio of Fe(II) in octahedral coordination to Fe(III) in both tetrahedral and  
165 octahedral coordination was further calculated from XMCD spectra by means of a nonlinear  
166 least-squares analysis as described previously.<sup>1,4,26</sup>

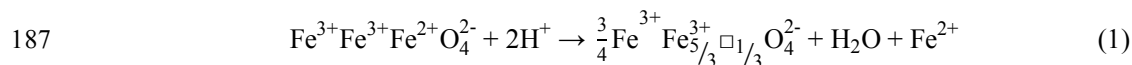
### 168 **3. Results and Discussion**

169 The XRD pattern (Fig. S1) showed that the synthetic NPs were pure magnetite, and the  
170 representative TEM images (Fig. S2) illustrated that they were  $\sim 10$  nm in size and nearly  
171 spherical in shape. The BET result indicated that the specific surface area of the synthetic NPs was  
172  $55.7$  m<sup>2</sup>/g. These characteristics are in good agreement with the properties of synthetic magnetite  
173 NPs reported in our previous studies.<sup>1,2,4</sup>

174

### 175 3.1. pH Effects on $\text{Fe}^{2+}_{(\text{aq})}$ -Magnetite Interaction.

176 Figure 1A shows  $\text{Fe}^{2+}_{(\text{aq})}$  release from magnetite as a function of time in suspensions of 695  
 177  $\text{mg L}^{-1}$  magnetite NPs ( $[\text{Fe}(\text{II})]$  equivalent = 3 mM) at pH 6 - 8 without amended  $\text{Fe}^{2+}_{(\text{aq})}$ . The  
 178 measured  $[\text{Fe}^{2+}_{(\text{aq})}]$  was nearly unchanged at pH 8 during the 24-hr experiment, but at pH 6 - 7  
 179  $[\text{Fe}^{2+}_{(\text{aq})}]$  gradually increased with time and reached a plateau ( $\sim 550 \mu\text{M}$  at pH 6 and  $\sim 250 \mu\text{M}$  at  
 180 pH 7) after about 120 minutes. The results indicate that more  $\text{Fe}^{2+}_{(\text{aq})}$  ions were released from  
 181 magnetite at a lower pH, which is consistent with the results of our previous study.<sup>1</sup> The stock  
 182 suspension of synthetic magnetite NPs naturally equilibrated to pH  $\sim 8.5$  after washing processes.<sup>26</sup>  
 183 When an aliquot of the stock suspension was spiked into the buffer solution at pH 6 or 7,  
 184 magnetite NPs were transferred from the stock suspension at pH  $\sim 8.5$  to a buffer solution at a  
 185 lower pH. The sudden pH decrease resulted in the release of  $\text{Fe}^{2+}_{(\text{aq})}$  from magnetite NPs  
 186 into the aqueous phase due to the proton-promoted dissolution, as described by the equation:<sup>1,31</sup>



188 The symbol  $\square$  represents a cationic vacancy due to diffusive migration of iron cations out of the  
 189 octahedral sublattice. When the NP stock suspension was added to the buffer solution at pH 8, the  
 190 pH change was insignificant, and accordingly a negligible amount of  $\text{Fe}^{2+}_{(\text{aq})}$  was released from  
 191 magnetite.

192 When the  $695 \text{ mg L}^{-1}$  magnetite suspension was added to the pH 6 - 8 buffer solutions  
 193 amended with  $1000 \mu\text{M Fe}^{2+}_{(\text{aq})}$ , the time-dependent concentrations of  $\text{Fe}^{2+}_{(\text{aq})}$  (Fig. 1B) were  
 194 obviously different from those without  $\text{Fe}^{2+}_{(\text{aq})}$  amendment (Fig. 1A). In the pH 6 buffer solution  
 195 amended with  $1000 \mu\text{M Fe}^{2+}_{(\text{aq})}$ , the values of  $[\text{Fe}^{2+}_{(\text{aq})}]$  increased with time and reached a stable

1  
2  
3  
4 196 value at  $\sim 1430 \mu\text{M}$  after  $\sim 60$  min. Considering  $1000 \mu\text{M Fe}^{2+}_{(\text{aq})}$  was initially added,  $430 \mu\text{M}$   
5  
6 197  $\text{Fe}^{2+}_{(\text{aq})}$  were released from  $695 \text{ mg L}^{-1}$  magnetite NPs under this condition, which was noticeably  
7  
8 198 less than the value ( $550 \mu\text{M}$ ) from magnetite without added  $\text{Fe}^{2+}_{(\text{aq})}$ . As indicated by Equation (1)  
9  
10  
11 199 and Le Chatelier's principle, increasing the initial concentration/activity of  $\text{Fe}^{2+}_{(\text{aq})}$  can inhibit the  
12  
13 200 extent of magnetite dissolution and thus decrease the amount of  $\text{Fe}^{2+}_{(\text{aq})}$  released from magnetite.

14  
15  
16 201 In the pH 7 buffer solution amended with  $1000 \mu\text{M Fe}^{2+}_{(\text{aq})}$ ,  $[\text{Fe}^{2+}_{(\text{aq})}]$  slightly decreased with  
17  
18 202 time and reached a stable value at  $\sim 900 \mu\text{M}$  after about 10 min (Fig. 1B), indicating the uptake of  
19  
20  
21 203  $\sim 100 \mu\text{M Fe}^{2+}_{(\text{aq})}$  by  $695 \text{ mg L}^{-1}$  magnetite NPs. Thus, the addition of  $1000 \mu\text{M Fe}^{2+}_{(\text{aq})}$  to the  $695$   
22  
23 204  $\text{mg L}^{-1}$  magnetite suspension at pH 7 changed the dominant reaction from  $\text{Fe}^{2+}_{(\text{aq})}$  release to  $\text{Fe}^{2+}_{(\text{aq})}$   
24  
25 205 uptake. At pH = 8,  $[\text{Fe}^{2+}_{(\text{aq})}]$  fluctuated around  $400 \mu\text{M}$  during the 24-hr experiment, suggesting an  
26  
27 206 instant uptake of  $\sim 600 \mu\text{M Fe}^{2+}_{(\text{aq})}$  by  $695 \text{ mg L}^{-1}$  magnetite NPs. The results indicate that the  
28  
29 207 presence of  $1000 \mu\text{M Fe}^{2+}_{(\text{aq})}$  inhibited Fe(II) release from magnetite at pH 6 and also promoted  
30  
31 208  $\text{Fe}^{2+}_{(\text{aq})}$  uptake at pH 7-8. The addition of  $1000 \mu\text{M Fe}^{2+}_{(\text{aq})}$  at pH 7 not only changed the dominant  
32  
33 209 interfacial reaction from  $\text{Fe}^{2+}_{(\text{aq})}$  release to  $\text{Fe}^{2+}_{(\text{aq})}$  uptake, but also shortened the time needed to  
34  
35 210 reach equilibrium from  $\sim 120$  min to  $\sim 60$  min (Fig. 1).

36  
37  
38  
39  
40  
41 211 Figure 1 also shows that, under the experimental conditions in this study, the concentrations  
42  
43 212 of  $\text{Fe}^{2+}_{(\text{aq})}$  reached a plateau in less than 24 hours. Previous studies also reported that the  
44  
45 213 suspensions of iron oxide, such as magnetite, hematite, and goethite, reached equilibrium after  
46  
47 214 24-hour reaction with  $\text{Fe}^{2+}_{(\text{aq})}$ .<sup>3, 32</sup> Thus, equilibrium concentrations of  $\text{Fe}^{2+}_{(\text{aq})}$  in magnetite  
48  
49 215 suspensions under different experimental conditions (pH = 6 - 8; initial  $\text{Fe}^{2+}_{(\text{aq})}$  concentrations = 0  
50  
51 216 -  $1000 \mu\text{M}$ ; NP loadings =  $300 - 3000 \mu\text{M}$  [Fe(II)] equivalent) were measured after 24-hour  
52  
53 217 reaction with  $\text{Fe}^{2+}_{(\text{aq})}$  (Fig. S3). To compare reaction extents in different experiments, the  
54  
55  
56  
57  
58  
59  
60

1  
2  
3  
4 218 difference between equilibrium concentration ( $[\text{Fe}^{2+}_{(\text{aq})}]_{\text{equilibrium}}$ ) and initial concentration  
5  
6 219 ( $[\text{Fe}^{2+}_{(\text{aq})}]_{\text{initial}}$ ) of  $\text{Fe}^{2+}_{(\text{aq})}$ , named as  $\Delta[\text{Fe}^{2+}_{(\text{aq})}]$  ( $\Delta[\text{Fe}^{2+}_{(\text{aq})}] = [\text{Fe}^{2+}_{(\text{aq})}]_{\text{equilibrium}} - [\text{Fe}^{2+}_{(\text{aq})}]_{\text{initial}}$ ), was  
7  
8 220 plotted as a function of NP loadings in Figure 2. Without added  $\text{Fe}^{2+}_{(\text{aq})}$ , the values of  $\Delta[\text{Fe}^{2+}_{(\text{aq})}]$  in  
9  
10  
11 221 the systems with a fixed magnetite loading showed the order: pH 6 > pH 7 > pH 8  $\approx$  0 (Fig. 2A).  
12  
13 222 As mentioned above, the lower pH facilitated proton-promoted dissolution of magnetite, resulting  
14  
15 223 in more  $\text{Fe}^{2+}_{(\text{aq})}$  released. Moreover, no matter how much  $\text{Fe}^{2+}_{(\text{aq})}$  was initially added or what  
16  
17 224 magnetite loading was used,  $\Delta[\text{Fe}^{2+}_{(\text{aq})}]$  was always positive at pH 6 (Fig. 2B), confirming that  
18  
19 225 proton-promoted dissolution was the dominant interfacial reaction at pH 6. On the contrary, at pH  
20  
21 226 8 and in the presence of added  $\text{Fe}^{2+}_{(\text{aq})}$ ,  $\Delta[\text{Fe}^{2+}_{(\text{aq})}]$  values were all negative, indicating that uptake  
22  
23 227 of  $\text{Fe}^{2+}_{(\text{aq})}$  by magnetite was the dominant interfacial reaction in the pH 8 buffer solution amended  
24  
25 228 with  $\text{Fe}^{2+}_{(\text{aq})}$  (Fig. 2D).  
26  
27  
28  
29  
30

31 229 The tipping point in  $\Delta[\text{Fe}^{2+}_{(\text{aq})}]$  in our system was found to coincide at pH 7, where  $\Delta[\text{Fe}^{2+}_{(\text{aq})}]$   
32  
33 230 could be positive or negative depending on magnetite loading and initial  $[\text{Fe}^{2+}_{(\text{aq})}]$  (Fig. 2C). The  
34  
35 231 results suggest that the dominant reaction between magnetite and  $\text{Fe}^{2+}_{(\text{aq})}$  at pH 7 could be  
36  
37 232 switched between  $\text{Fe}^{2+}_{(\text{aq})}$  release and  $\text{Fe}^{2+}_{(\text{aq})}$  uptake simply by changing the ratio of initial  $[\text{Fe}^{2+}_{(\text{aq})}]$   
38  
39 233 ( $C_0$ ) to magnetite loading ( $C_{\text{Mt}}$ ). When the  $C_0/C_{\text{Mt}}$  ratio was less than  $\sim 0.5$ ,  $\text{Fe}^{2+}_{(\text{aq})}$  release from  
40  
41 234 magnetite NPs was the dominant reaction (Fig. 3). Otherwise,  $\text{Fe}^{2+}_{(\text{aq})}$  uptake was more favorable.  
42  
43  
44 235 The potential explanation for the reversible direction of electron equivalents ( $\text{Fe}^{2+}_{(\text{aq})}$ ) across the  
45  
46 236 magnetite-solution interface at pH 7 will be discussed in section 3.4. The change of interfacial  
47  
48 237 reactions in the range of pH 6 - 8 indicates that solution pH can significantly impact the  
49  
50 238 distribution of electron equivalents between solution and magnetite, influencing the reductive  
51  
52 239 reactivity of magnetite NPs.  
53  
54  
55  
56  
57  
58  
59  
60

### 240 **3.2. Effects of NP Loading and Initial $[\text{Fe}^{2+}_{(\text{aq})}]$ on $\text{Fe}^{2+}_{(\text{aq})}$ -Magnetite Interaction.**

241 When pH and initial  $[\text{Fe}^{2+}_{(\text{aq})}]$  were same, the absolute values of  $\Delta[\text{Fe}^{2+}_{(\text{aq})}]$  increased linearly  
242 with the increase of magnetite loading from 300 to 3000  $\mu\text{M}$  at pH 6 and pH 8 (Figure 2). As  
243 discussed above, the dominant reaction at pH 6 was proton-promoted dissolution of magnetite,  
244 which involves the initial binding of protons to surface oxygen atoms, weakening bridging Fe-O  
245 bonds, and the detachment of Fe(II) from the magnetite surface into solution.<sup>33</sup> Increasing  
246 magnetite loading can effectively elevate the concentration of Fe(II) introduced into the system in  
247 the form of NPs, which on the basis of Equation 1 shifts the equilibrium to the right, resulting in  
248 more  $\text{Fe}^{2+}_{(\text{aq})}$  released and the greater values of  $\Delta[\text{Fe}^{2+}_{(\text{aq})}]$  (Fig. 2B). As pH increased from 6 to 8,  
249 conversely the decreased acidity causes an equilibrium shift in the opposite direction whereupon  
250 the dominant reaction becomes  $\text{Fe}^{2+}_{(\text{aq})}$  uptake, which begins with the adsorption of  $\text{Fe}^{2+}_{(\text{aq})}$  onto  
251 magnetite surface, followed by interfacial electron transfer between sorbed Fe(II) and structural  
252 Fe(III).<sup>34</sup> Under this condition, the higher magnetite loading provided more active surface sites for  
253  $\text{Fe}^{2+}_{(\text{aq})}$  adsorption and accordingly promoted  $\text{Fe}^{2+}_{(\text{aq})}$  uptake. As a result, the absolute values of  
254  $\Delta[\text{Fe}^{2+}_{(\text{aq})}]$  were higher, as more magnetite NPs were added to the solution at pH 8 (Fig. 2D).  
255 Although increasing NP concentrations could change aggregation state of NPs, the continuous  
256 shaking in all experiments promoted the diffusion of  $\text{Fe}^{2+}_{(\text{aq})}$  onto magnetite surface and  
257 minimized the impact of NP aggregation on  $\text{Fe}^{2+}_{(\text{aq})}$ -magnetite interaction.

258 In all experiments,  $\Delta[\text{Fe}^{2+}_{(\text{aq})}]$  was linearly proportional to magnetite loading (Fig. 2). Table  
259 S2 shows the functions and R-squared values of all fitted regression lines in Figure 2. The slopes  
260 of the fitted lines at pH 6 varied between 0.1455 and 0.1639 were independent of the  
261 concentration of added  $\text{Fe}^{2+}_{(\text{aq})}$ . Compared to the slopes at pH 6, the absolute values of the

1  
2  
3  
4 262 corresponding slopes at pH 8 were obviously smaller (Table S2). The difference might imply that  
5  
6 263 the influence of NP loading was more significant on magnetite dissolution than on  $\text{Fe}^{2+}_{(\text{aq})}$  uptake  
7  
8 264 by magnetite. The high R-squared values in all experiments confirmed the linear relationship  
9  
10  
11 265 between  $\Delta[\text{Fe}^{2+}_{(\text{aq})}]$  and magnetite loading, indicating that  $\text{Fe}^{2+}_{(\text{aq})}$ -magnetite interaction under all  
12  
13 266 of these conditions was a surface-mediated process, presumably limited by available specific  
14  
15  
16 267 surface area. Aggregation state of magnetite was unlikely to significantly change as pH increased  
17  
18 268 from 6 to 8, because extensive aggregation of magnetite NPs occurred at all these pH values due  
19  
20  
21 269 to a combination of Lifschitz–van der Waals and magnetic forces,<sup>35</sup> as well as the weak  
22  
23 270 electrostatic repulsion between magnetite NPs at pH 6-8.<sup>36</sup> Thus, the observed pH effects on  
24  
25  
26 271  $\text{Fe}^{2+}_{(\text{aq})}$ -magnetite interaction could not be attributed to pH-dependent aggregation behavior of  
27  
28 272 NPs.

29  
30 273 To illustrate the effect of initial  $[\text{Fe}^{2+}_{(\text{aq})}]$  on magnetite- $\text{Fe}^{2+}_{(\text{aq})}$  interaction,  $\Delta[\text{Fe}^{2+}_{(\text{aq})}]$  was  
31  
32 274 replotted versus the initial concentration of added  $\text{Fe}^{2+}_{(\text{aq})}$  ( $[\text{Fe}^{2+}_{(\text{aq})}]_{\text{add}}$ ) (Fig. S4). When NP  
33  
34 275 loading and pH were fixed, there is a linear relationship between  $\Delta[\text{Fe}^{2+}_{(\text{aq})}]$  and  $[\text{Fe}^{2+}_{(\text{aq})}]_{\text{add}}$  under  
35  
36 276 all experimental conditions in this study. At pH 6, the decrease in  $\Delta[\text{Fe}^{2+}_{(\text{aq})}]$  with increasing  
37  
38 277  $[\text{Fe}^{2+}_{(\text{aq})}]_{\text{add}}$  suggests the inhibition of magnetite dissolution by the additional  $\text{Fe}^{2+}_{(\text{aq})}$ , as discussed  
39  
40  
41 278 above. In contrast, at pH 8, the higher initial  $[\text{Fe}^{2+}_{(\text{aq})}]$  led to the greater absolute values of  
42  
43 279  $\Delta[\text{Fe}^{2+}_{(\text{aq})}]$ , indicating that the more added  $\text{Fe}^{2+}_{(\text{aq})}$  promoted  $\text{Fe}^{2+}_{(\text{aq})}$  uptake by magnetite NPs. As  
44  
45  
46 280 mentioned above, the adsorption of  $\text{Fe}^{2+}_{(\text{aq})}$  onto magnetite surface is a key step to initiate  $\text{Fe}^{2+}_{(\text{aq})}$   
47  
48 281 uptake by magnetite. Increasing the concentration of added  $\text{Fe}^{2+}_{(\text{aq})}$  could facilitate the adsorption  
49  
50  
51 282 of  $\text{Fe}^{2+}_{(\text{aq})}$  on magnetite surface. Moreover, in thermodynamic terms, increasing concentration of  
52  
53  
54 283  $\text{Fe}^{2+}_{(\text{aq})}$  resulted in the lower reduction potential of aqueous solution. The difference in redox  
55  
56  
57  
58  
59  
60

1  
2  
3  
4 284 potentials between magnetite and solution tends to drive  $\text{Fe}^{2+}_{(\text{aq})}$  uptake by magnetite, in order to  
5  
6 285 establish a new equilibrium at the solid/solution interface. Thus, the higher  $[\text{Fe}^{2+}_{(\text{aq})}]_{\text{add}}$  promoted  
7  
8 286  $\text{Fe}^{2+}_{(\text{aq})}$  uptake by magnetite NPs.  
9

10  
11  
12 287

### 15 288 **3.3. Structural Fe(II)/Fe(III) Response.**

16  
17  
18 289 The extent to which this  $\text{Fe}^{2+}_{(\text{aq})}$  uptake and release by magnetite involves corresponding  
19  
20 290 changes in structural Fe(II)/Fe(III) in the bulk was evaluated by performing  $\mu\text{XRD}$  measurements.  
21  
22  
23 291 As shown in Figure S5, the only crystalline phase observed in all  $\mu\text{XRD}$  patterns of post-reaction  
24  
25 292 NPs was magnetite. Based on the known smooth relationship between cubic unit-cell length and  
26  
27  
28 293 magnetite stoichiometry, the structural Fe(II)/Fe(III) ratio in magnetite NPs was estimated directly  
29  
30 294 from the measured cell parameter according to the method reported in previous studies.<sup>26, 37</sup> The  
31  
32  
33 295 structural Fe(II)/Fe(III) ratios calculated from the  $\mu\text{XRD}$  patterns of  $695 \text{ mg L}^{-1}$  magnetite NPs  
34  
35 296 ( $[\text{Fe(II)}]$  equivalent =  $3000 \mu\text{M}$ ) before and after reactions with  $1000 \mu\text{M Fe}^{2+}_{(\text{aq})}$  at pH 6 - 8 were  
36  
37  
38 297 shown in Figure 4 and Table 1. The results indicate that, irrespective of whether  $\text{Fe}^{2+}_{(\text{aq})}$  was  
39  
40 298 initially added, the structural Fe(II)/Fe(III) ratio in the magnetite suspensions with the same initial  
41  
42  
43 299  $[\text{Fe}^{2+}_{(\text{aq})}]$  and magnetite loading increased from pH 6 to pH 8. For example, at pH 8 without added  
44  
45 300  $\text{Fe}^{2+}_{(\text{aq})}$ , the Fe(II)/Fe(III) ratio of magnetite NPs was 0.526 and obviously larger than the ratio  
46  
47  
48 301 (0.478) at pH 6 and that (0.498) at pH 7. This is consistent with the results, shown in Figure 2, that  
49  
50 302 low pH facilitates magnetite dissolution and  $\text{Fe}^{2+}_{(\text{aq})}$  release from magnetite, whereas no detectable  
51  
52  
53 303  $\text{Fe}^{2+}_{(\text{aq})}$  was released from magnetite at pH 8. Moreover, the addition of  $1000 \mu\text{M Fe}^{2+}_{(\text{aq})}$  at pH 6 -  
54  
55 304 8 resulted in the higher structural Fe(II)/Fe(III) ratio, compared to the ratio of samples without  
56  
57  
58  
59  
60



1  
2  
3  
4 305 added  $\text{Fe}^{2+}_{(\text{aq})}$ . The trend agrees well with the results that  $\text{Fe}^{2+}_{(\text{aq})}$  amendment inhibited  $\text{Fe}^{2+}_{(\text{aq})}$   
5  
6 306 release from magnetite at low pH and promoted  $\text{Fe}^{2+}_{(\text{aq})}$  uptake by magnetite at high pH (Fig. 2).  
7  
8 307 The  $\text{Fe}^{2+}$  content in the solid is thus highly mobile and responsive to changes in chemical potential  
9  
10  
11 308 at the magnetite-solution interface.  
12  
13

14 309 It is worth mentioning that under some conditions a hyperstoichiometric “cation-excess”  
15  
16 310 magnetite was formed. For example, at pH 8, the addition of 1000  $\mu\text{M}$   $\text{Fe}^{2+}_{(\text{aq})}$  increased the  
17  
18 311 structural Fe(II)/Fe(III) ratio well beyond 0.5 (Table 1). The exact physical nature of this condition  
19  
20 312 remains unclear. In previous studies, uptake of  $\text{Fe}^{2+}_{(\text{aq})}$  by magnetite NPs at elevated pH has been  
21  
22 313 simply attributed to the increasing adsorption capacity for  $\text{Fe}^{2+}_{(\text{aq})}$ . The point of zero charge of  
23  
24 314 magnetite is 6.4 - 6.85,<sup>14, 36, 38</sup> so increasing pH from 6 to 8 can lead to more negative surface that  
25  
26 315 might adsorb more  $\text{Fe}^{2+}_{(\text{aq})}$  non-specifically via electrostatic attraction.<sup>14</sup> However, Gorski et al.  
27  
28 316 (2009) reported that no stable sorbed Fe(II) species was observed on magnetite NPs after exposure  
29  
30 317 to  $\text{Fe}^{2+}_{(\text{aq})}$  at pH 7.2. They further showed that  $\text{Fe}^{2+}_{(\text{aq})}$  can incorporate into the structure of partially  
31  
32 318 oxidized or nonstoichiometric magnetite, and the extent of  $\text{Fe}^{2+}_{(\text{aq})}$  uptake is limited by the  
33  
34 319 formation of stoichiometric magnetite (Fe(II)/Fe(III) = 0.5). This conclusion was based on the  
35  
36 320 experiments with a constant magnetite loading (1 g/L) at pH 7.2. The results of the present study  
37  
38 321 indicate that increasing pH or initial  $[\text{Fe}^{2+}_{(\text{aq})}]$  can promote  $\text{Fe}^{2+}_{(\text{aq})}$  uptake and result in a  
39  
40 322 Fe(II)/Fe(III) beyond 0.5. This hyperstoichiometry may possibly indicate incorporation of ferrous  
41  
42 323 ions into minor cation vacancies in the octahedral sublattice, or the reduction of octahedral Fe(III)  
43  
44 324 by injected electrons from sorbed Fe(II).<sup>27, 39</sup>  
45  
46  
47  
48  
49  
50  
51  
52  
53

54 325 In addition to the structural Fe(II)/Fe(III) ratio in the bulk as shown by  $\mu\text{XRD}$ , the  
55  
56 326 Fe(II)/Fe(III) ratio in the near-surface region was independently probed using Fe L-edge XAS and  
57  
58  
59  
60

1  
2  
3  
4 327 XMCD (Fig. 5 and Table 1). In contrast to  $\mu$ XRD, the information depth of XAS/XMCD is no  
5  
6 328 more than 4.5 nm, with sensitivity that exponentially increases to the outermost surface atoms.  
7  
8 329 Furthermore, whereas XAS detects all iron within this near-surface region, XMCD is sensitive  
9  
10 330 only to the magnetically ordered Fe(II) and Fe(III), thus selecting primarily for iron sites in lattice  
11  
12 331 positions at the surface.<sup>28</sup> When 695 mg L<sup>-1</sup> magnetite NPs were exposed to the pH 7 buffer  
13  
14 332 solution without Fe<sup>2+</sup><sub>(aq)</sub> amendment, the surface Fe(II)/Fe(III) ratio increased from 0.538 to 0.604,  
15  
16 333 while the structural Fe(II)/Fe(III) ratio decreased from 0.544 to 0.498 (Table 1). The opposite  
17  
18 334 trends likely indicate solid-state migration of electrons from the interior to the near-surface region,  
19  
20 335 as has been previously observed during the acidic dissolution of magnetite NPs and  
21  
22 336 microparticles.<sup>4, 26, 28</sup>

23  
24  
25  
26  
27  
28 337 When 500  $\mu$ M Fe<sup>2+</sup><sub>(aq)</sub> were initially added at pH 7,  $\Delta$ [Fe<sup>2+</sup><sub>(aq)</sub>] was 150  $\mu$ M, indicating that  
29  
30 338 magnetite dissolution was the dominant reaction. However, the surface-localized Fe(II)/Fe(III)  
31  
32 339 ratio became 0.754 that was evidently higher than the ratios of magnetite in the stock suspension  
33  
34 340 (0.538) or in the pH 7 buffer solution without added Fe<sup>2+</sup><sub>(aq)</sub> (0.604) (Table 1). The presence of  
35  
36 341 500  $\mu$ M Fe<sup>2+</sup><sub>(aq)</sub> worked against proton-promoted dissolution of magnetite, and the Fe<sup>2+</sup><sub>(aq)</sub>  
37  
38 342 amendment induces further enrichment of Fe(II) in the near-surface region. When the  
39  
40 343 concentration of Fe<sup>2+</sup><sub>(aq)</sub> was increased to 1000  $\mu$ M,  $\Delta$ [Fe<sup>2+</sup><sub>(aq)</sub>] decreased from 150 to 19  $\mu$ M,  
41  
42 344 indicating a stronger inhibition of dissolution. However, the surface-localized Fe(II)/Fe(III) ratio  
43  
44 345 was no longer observed to increase by XMCD, suggesting that the limit for Fe(II) enrichment into  
45  
46 346 surface structure had been reached. Once saturated, the relatively high surface-localized  
47  
48 347 Fe(II)/Fe(III) ratio might also suggest that further participation of Fe(II) from particle interiors in  
49  
50 348 interfacial electron transfer may also saturate.  
51  
52  
53  
54  
55  
56  
57  
58  
59  
60

1  
2  
3  
4 349 At pH 8, the surface-localized Fe(II)/Fe(III) ratio of magnetite NPs was also in the order:  
5  
6 350 stock suspension < buffer solution without added  $\text{Fe}^{2+}_{(\text{aq})}$  < buffer solution with 1000  $\mu\text{M}$   $\text{Fe}^{2+}_{(\text{aq})}$ .  
7  
8 351 When NPs were exposed to the pH 8 buffer solution without additional  $\text{Fe}^{2+}_{(\text{aq})}$ , no measurable  
9  
10 352  $\text{Fe}^{2+}_{(\text{aq})}$  was released from NPs, but the structural Fe(II)/Fe(III) ratio decreased from 0.544 to 0.526  
11  
12 353 as shown in Table 1. Simultaneously, the surface-localized Fe(II)/Fe(III) ratio of magnetite NPs  
13  
14 354 increased from 0.538 to 0.593. Although no change in the concentration of  $\text{Fe}^{2+}_{(\text{aq})}$  was observed  
15  
16 355 under this condition, Fe(II) enriched at the near-surface region of magnetite NPs as a result of  
17  
18 356 transferring NPs from the stock suspension to the pH 8 buffer solution. When 1000  $\mu\text{M}$   $\text{Fe}^{2+}_{(\text{aq})}$   
19  
20 357 was added at pH 8, the structural Fe(II)/Fe(III) ratio increased from 0.526 to 0.538, and the  
21  
22 358 surface-localized Fe(II)/Fe(III) ratio increased from 0.593 to 0.610 (Table 1). The results might  
23  
24 359 suggest that  $\text{Fe}^{2+}_{(\text{aq})}$  incorporation or electron injection occurred both at the near-surface region  
25  
26 360 and in particle interiors under this condition, resulting in the distribution of excess Fe(II)  
27  
28 361 throughout the hyperstoichiometric magnetite NPs. In the XAS in general, the  $L_{2,3}$ -edge for Fe  
29  
30 362 exhibits a shift to higher energy with an increase in oxidation state. Figure 6 shows that the lower  
31  
32 363 energy Fe  $L_{2,3}$ -edge peak intensity at 707.8 eV increased as  $\text{Fe}^{2+}_{(\text{aq})}$  was added, corresponding to  
33  
34 364 an increase the total ferrous Fe concentration at the surface of the NPs. The increase in intensity of  
35  
36 365 the first peak ( $\sim 707.8$  eV) in XMCD spectrum in Figure 5 corresponds to Fe(II) in octahedral  
37  
38 366 coordination and demonstrates that the high Fe(II)/Fe(III) is truly a gradient within the magnetite  
39  
40 367 structure. If the Fe(II) was surface sorbed in a non-specific or poorly ordered manner, it would be  
41  
42 368 detectable by an increase in the low energy peak intensity in the XA without a corresponding  
43  
44 369 increase in the first peak in the XMCD. Moreover, no secondary crystalline phases were observed  
45  
46 370 by  $\mu\text{XRD}$  in all samples after reaction with  $\text{Fe}^{2+}_{(\text{aq})}$ . Thus, the higher Fe(II)/Fe(III) ratio shown in  
47  
48  
49  
50  
51  
52  
53  
54  
55  
56  
57  
58  
59  
60

1  
2  
3  
4 371 XMCD spectra can be attributed to changes in the composition of the structural iron at the  
5  
6 372 near-surface after reaction, and not to secondary phases or adsorbed iron complexes.  
7

8  
9 373  
10

#### 11 12 374 **3.4. Redistribution of Fe(II) as a Result of Fe<sup>2+</sup><sub>(aq)</sub>-Magnetite Interaction.** 13

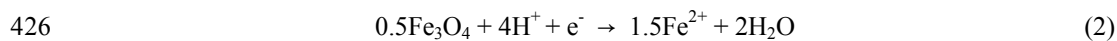
14  
15 375 Attempts were made to quantify the mass and electron balanced redistribution of Fe(II)  
16  
17 376 between the aqueous phase, particle interiors, and particle surfaces, as a function of system  
18  
19 377 variables, based on the results of this study. For example,  $\mu$ XRD results showed that the  
20  
21 378 Fe(II)/Fe(III) ratio of magnetite in the stock suspension of synthetic NPs was 0.544 (Table 1).  
22  
23 379 When the magnetite loading was 695 mg L<sup>-1</sup> ([Fe(II)] equivalent = 3 mM), the concentrations of  
24  
25 380 structural Fe(II) and Fe(III) in as-synthesized magnetite NPs were 3000  $\mu$ M and 5516  $\mu$ M,  
26  
27 381 respectively (Table 2). After exposed to the pH 7 buffer solution without added Fe<sup>2+</sup><sub>(aq)</sub>, the  
28  
29 382 Fe(II)/Fe(III) ratio of magnetite decreased to 0.498, and  $\Delta$ [Fe<sup>2+</sup><sub>(aq)</sub>] was 250  $\mu$ M. As mentioned  
30  
31 383 above, no stable sorbed Fe(II) species were observed on NP surfaces after reaction with Fe<sup>2+</sup><sub>(aq)</sub> at  
32  
33 384 pH 7,<sup>3</sup> and no secondary crystalline phase was observed in the  $\mu$ XRD patterns of post-reaction  
34  
35 385 samples. Thus,  $\Delta$ [Fe<sup>2+</sup><sub>(aq)</sub>] in solution presumably equaled the decrease of total Fe concentration  
36  
37 386 ([Fe<sub>tot</sub>]) in NPs at equilibrium. As 250  $\mu$ M Fe<sup>2+</sup><sub>(aq)</sub> ( $\Delta$ [Fe<sup>2+</sup><sub>(aq)</sub>] = 250  $\mu$ M) was released from 695  
38  
39 387 mg L<sup>-1</sup> magnetite NPs after the NPs were transferred from the stock suspension to the pH 7 buffer  
40  
41 388 solution, the total Fe ([Fe<sub>tot</sub>]) in the magnetite NPs accordingly decreased from 8516 to 8266  $\mu$ M  
42  
43 389 (Table 2). The  $\mu$ XRD results show that the structural Fe(II)/Fe(III) ratio of magnetite NPs was  
44  
45 390 0.498 in the pH 7 buffer solution without amended Fe<sup>2+</sup><sub>(aq)</sub> (Table 1), so the concentration of Fe(II)  
46  
47 391 in magnetite structure was 2748  $\mu$ M that was 252  $\mu$ M less than the structural Fe(II) concentration  
48  
49  
50  
51  
52  
53  
54  
55  
56  
57  
58  
59  
60

1  
2  
3  
4 392 (3000  $\mu\text{M}$ ) in  $695 \text{ mg L}^{-1}$  as-synthesized magnetite NPs (Table 2). The results indicate that the  
5  
6 393 increase of  $\text{Fe}^{2+}_{(\text{aq})}$  concentration ( $\Delta[\text{Fe}^{2+}_{(\text{aq})}]$ ) from chemical analysis was very close to the  
7  
8 394 decrease of structural Fe(II) in magnetite NPs ( $\Delta[\text{Fe(II)}_{\text{str}}]$ ) measured by  $\mu\text{XRD}$ . The good  
9  
10 395 consistency confirmed that, at pH 7 and without added  $\text{Fe}^{2+}_{(\text{aq})}$ , the increase of  $[\text{Fe}^{2+}_{(\text{aq})}]$  in solution  
11  
12  
13 396 was mainly attributed to Fe(II) release from magnetite structure. Moreover, the concentration of  
14  
15  
16 397 structural Fe(III) in magnetite was nearly unchanged after reaction under this condition.

17  
18  
19 398 However, when  $1000 \mu\text{M Fe}^{2+}_{(\text{aq})}$  was initially added in pH 7 buffer solution,  $\Delta[\text{Fe}^{2+}_{(\text{aq})}]$  was  
20  
21 399 only  $19 \mu\text{M}$ , indicating the corresponding total Fe in NPs was  $8497 \mu\text{M}$ . The  $\mu\text{XRD}$  results  
22  
23  
24 400 showed the Fe(II)/Fe(III) ratio of NPs in this case was 0.511, so the concentrations of structural  
25  
26 401 Fe(II) and Fe(III) were  $2874 \mu\text{M}$  and  $5623 \mu\text{M}$ , respectively. Compared to as-synthesized NPs, the  
27  
28  
29 402 equivalent concentration of structural Fe(II) decreased  $126 \mu\text{M}$ , but that of structural Fe(III)  
30  
31 403 increased  $107 \mu\text{M}$  (Table 2). This suggests that charge redistribution between Fe(II) and Fe(III) in  
32  
33  
34 404 the magnetite structure might happen concurrently with proton-promoted dissolution in the pH 7  
35  
36 405 buffer solution amended with  $1000 \mu\text{M Fe}^{2+}_{(\text{aq})}$ . The calculation above was based on the  
37  
38  
39 406 assumption that there were negligible amounts of amorphous iron-containing solid phase formed  
40  
41 407 in the system at equilibrium. Although the  $\mu\text{XRD}$  and XMCD results in this study could not rule  
42  
43  
44 408 out the formation of iron-containing amorphous phases, the representative TEM image of  
45  
46 409 magnetite NPs after reaction with  $\text{Fe}^{2+}_{(\text{aq})}$  at pH 7 (Figure S6) did not show the presence of  
47  
48  
49 410 amorphous phases. Moreover, previous experimental studies have suggested that no stable,  
50  
51 411 adsorbed iron complexes or phases on iron oxide surfaces after reaction with  $\text{Fe}^{2+}_{(\text{aq})}$  under  
52  
53 412 anaerobic conditions at pH 7.<sup>3, 21, 22, 25, 33, 39-41</sup> Nevertheless, more detailed studies on iron  
54  
55  
56 413 speciation as a result of magnetite-  $\text{Fe}^{2+}_{(\text{aq})}$  interaction under different experimental conditions are

1  
2  
3  
4 414 needed, in order to precisely describe the distribution of Fe(II) and electrons at the interface  
5  
6 415 between magnetite and  $\text{Fe}^{2+}_{(\text{aq})}$ .  
7  
8

9 416 The findings in this study showed that  $\text{Fe}^{2+}_{(\text{aq})}$  uptake or release can occur in the  
10  
11 417  $\text{Fe}^{2+}_{(\text{aq})}$ -magnetite system depending on pH, initial  $\text{Fe}^{2+}_{(\text{aq})}$  concentration, and NP loading. The  
12  
13  
14 418 flow direction of electron equivalents in the form of Fe(II) across the  $\text{Fe}^{2+}_{(\text{aq})}$ -magnetite interface  
15  
16  
17 419 can be determined by the difference in redox potentials between magnetite and solution. For  
18  
19 420 example, when 800  $\mu\text{M}$  magnetite NPs equilibrated with the pH 7 buffer solution amended with  
20  
21 421 750  $\mu\text{M}$   $\text{Fe}^{2+}_{(\text{aq})}$ ,  $\Delta[\text{Fe}^{2+}_{(\text{aq})}]$  was 3.1  $\mu\text{M}$  that was close to zero (Fig. 2C). The change of structural  
22  
23  
24 422 Fe(II)/Fe(III) in magnetite under this condition was negligible. Because the redox potentials of  
25  
26  
27 423 magnetite and solution must equal to each other at equilibrium, the redox potential of 800  $\mu\text{M}$   
28  
29 424 magnetite at pH 7 can be estimated from the equilibrium concentration of  $\text{Fe}^{2+}_{(\text{aq})}$ .<sup>32</sup> The  
30  
31 425 half-reaction between  $\text{Fe}^{2+}_{(\text{aq})}$  and magnetite can be written as:<sup>42</sup>  
32  
33



37  
38 427 By assuming that the activities of water and magnetite are 1, at room temperature (298 K), the  
39  
40 428 corresponding Nernst equation can be written as follows:  
41  
42

43 429 
$$E_{\text{H}} = E_{\text{H}}^0 - 88.5 \log\{\text{Fe}^{2+}_{(\text{aq})}\} - 236 \text{ pH} \quad (3)$$
  
44  
45

46 430 where  $E_{\text{H}}^0$  equals 1090 mV vs SHE;<sup>42</sup>  $\{\text{Fe}^{2+}_{(\text{aq})}\}$  is the activity of  $\text{Fe}^{2+}_{(\text{aq})}$  at equilibrium;  $E_{\text{H}}$  is  
47  
48  
49 431 the reduction potential of magnetite suspension with  $\text{Fe}^{2+}_{(\text{aq})}$  at a given pH. Thus, the redox  
50  
51 432 potential of 800  $\mu\text{M}$  magnetite NPs at pH 7 was close to -266 mV. When the initial  $[\text{Fe}^{2+}_{(\text{aq})}]$   
52  
53  
54 433 increased from 750 to 1000  $\mu\text{M}$ , the calculated  $E_{\text{H}}$  value of solution according to equation (3) was  
55  
56 434 lower than -266 mV. To reach equilibrium under this condition,  $\text{Fe}^{2+}_{(\text{aq})}$  uptake happened, in order  
57  
58  
59  
60

1  
2  
3  
4 435 to decrease  $\text{Fe}^{2+}_{(\text{aq})}$  concentration and correspondingly increase  $E_{\text{H}}$  of solution. Because redox  
5  
6 436 potential of magnetite is inversely proportional to structural Fe(II)/Fe(III) ratio in magnetite,  
7  
8 437  $\text{Fe}^{2+}_{(\text{aq})}$  uptake by magnetite could increase structural Fe(II)/Fe(III) ratio and also decrease redox  
9  
10  
11 438 potential of magnetite NPs. Therefore, the flow of electron equivalents from solution to magnetite  
12  
13 439 could effectively reduce the difference in the redox potentials between solution and magnetite,  
14  
15  
16 440 until a new equilibrium was reached. On the other hand, increasing magnetite loading can lead to a  
17  
18 441 lower reduction potential of magnetite suspension.<sup>15</sup> When magnetite loading was higher than 800  
19  
20 442  $\mu\text{M}$  at pH 7 and with 750  $\mu\text{M}$  added  $\text{Fe}^{2+}_{(\text{aq})}$ , the redox potential of magnetite was lower than -266  
21  
22  
23 443 mV. In this case,  $\text{Fe}^{2+}_{(\text{aq})}$  release from magnetite to solution could minimize the difference in redox  
24  
25  
26 444 potentials between magnetite NPs and aqueous solution. The findings in this study suggest that the  
27  
28 445 subtle alteration of solution conditions or magnetite loading may disrupt the equilibrium at the  
29  
30 446 magnetite-solution interface and drive the redistribution of Fe(II), in the form of  $\text{Fe}^{2+}_{(\text{aq})}$  release or  
31  
32  
33 447 uptake, until a new equilibrium is reached. The dynamic redistribution of electron equivalents also  
34  
35  
36 448 produces a challenge to experimentally quantify the reduction potential of magnetite NPs, which  
37  
38 449 can be quite distinct under different solution conditions or particle loadings.  
39  
40  
41  
42  
43

440

#### 451 **4. Conclusions**

452 Magnetite, as a common iron oxide in the environment with high reactivity and good  
453 biocompatibility, has been widely studied in a variety of environmental contexts and applications.  
454 The coexistence of magnetite and  $\text{Fe}^{2+}_{(\text{aq})}$  is pervasive in anoxic aquifers, resulting from various  
455 biogeochemical processes. Moreover, recharging magnetite with  $\text{Fe}^{2+}_{(\text{aq})}$  has been considered as an

1  
2  
3  
4 456 efficient way to trigger or enhance its reactivity in environmental remediation. This study presents  
5  
6 457 the first systematic work examining the effects of pH, initial  $\text{Fe}^{2+}_{(\text{aq})}$  concentration, and magnetite  
7  
8 458 loading on the distribution of electron equivalents in terms of Fe(II) between  $\text{Fe}^{2+}_{(\text{aq})}$  and  
9  
10 459 magnetite NPs at circumneutral pH. Increasing pH from 6 to 8 changed the primary reaction  
11  
12  
13 460 between magnetite NPs and  $\text{Fe}^{2+}_{(\text{aq})}$  from proton-promoted dissolution to  $\text{Fe}^{2+}_{(\text{aq})}$  uptake, which is  
14  
15 461 accompanied by an increase of the bulk structural Fe(II)/Fe(III) ratio in magnetite NPs.  $\text{Fe}^{2+}_{(\text{aq})}$   
16  
17 462 amendments inhibit magnetite dissolution at pH 6 and promote  $\text{Fe}^{2+}_{(\text{aq})}$  uptake at elevated pH,  
18  
19  
20 463 whereas the addition of more magnetite NPs can lead to  $\text{Fe}^{2+}_{(\text{aq})}$  release and uptake through shifts  
21  
22  
23 464 in the balance between two effects - increasing the available  $\text{Fe}^{2+}$  in the system while also  
24  
25 465 increasing the solid specific surface area.

26  
27  
28  
29 466 The findings in this study show that the reversible  $\text{Fe}^{2+}_{(\text{aq})}$  uptake/release by magnetite NPs  
30  
31 467 can be controlled by altering environmental variables, such as solution pH,  $\text{Fe}^{2+}_{(\text{aq})}$  concentration,  
32  
33 468 or magnetite loading. This study underscores the ability of magnetite to act as a rechargeable  
34  
35  
36 469 “battery” that couples to the redox-cycling of elements and transformation of contaminants in  
37  
38 470 redox-oscillating environments. This role for magnetite appears to promote microbial respiration<sup>43</sup>  
39  
40  
41 471 and stimulate direct interspecies electron transfer (DIET) in syntrophic microbial communities.<sup>36</sup>  
42  
43 472 Thus, the changes of surface-localized and structural Fe(II)/Fe(III) ratios as a result of  
44  
45 473  $\text{Fe}^{2+}_{(\text{aq})}$ -magnetite interaction under varied environmental conditions may also impact the related  
46  
47  
48 474 microbial metabolisms.

49  
50  
51 475 The stoichiometry and reduction reactivity of magnetite NPs can be substantially altered due  
52  
53  
54 476 to slight changes of environmental conditions. The results of this study also provide insights into  
55  
56 477 the variable reactivity of magnetite NPs in natural environments and provide a foundation for  
57  
58  
59  
60



1  
2  
3  
4 478 tailoring magnetite reactivity in NPs or as coatings on zero-valent iron (ZVI) for environmental  
5  
6 479 remediation.  
7  
8

9 480  
10  
11

12 481 **Conflicts of interest**  
13  
14

15 482 There are no conflicts of interest to declare.  
16  
17

18 483  
19  
20

21 484 **Acknowledgements**  
22  
23

24 485 This work was financially supported by National Basic Research Program of China (973 Program,  
25

26 486 2014CB846001) and National Natural Science Foundation of China (41472306, 41230103, and  
27

28 487 21375120). KMR acknowledges support from the U.S. Department of Energy (DOE), Office of  
29  
30

31 488 Science, Office of Basic Energy Sciences, from the Chemical Sciences, Geosciences, and  
32  
33

34 489 Biosciences Division through its Geosciences program at Pacific Northwest National Laboratory  
35

36 490 (PNNL). A portion of this research was performed using EMSL, a national scientific user facility  
37  
38

39 491 sponsored by the DOE Office of Biological and Environmental Research and located at PNNL.  
40

41 492 The work performed at the ALS is supported by the Director, Office of Basic Energy Sciences of  
42

43 493 the U.S. DOE under Contract No. DE-AC02-05CH11231. We thank Dr. Xin Zhang at PNNL for  
44  
45

46 494 taking TEM images of magnetite NPs.  
47  
48  
49  
50  
51  
52  
53  
54  
55  
56  
57  
58  
59  
60

1  
2  
3  
4 495 Table 1 The change of  $\text{Fe}^{2+}_{(\text{aq})}$  concentration ( $\Delta[\text{Fe}^{2+}_{(\text{aq})}]$ ), the structural Fe(II)/Fe(III) ratio in  
5  
6 496 magnetite NPs calculated from  $\mu\text{XRD}$  results, and the surface-localized XMCD Fe(II)/Fe(III)  
7  
8 497 ratio in magnetite NPs before and after reaction with  $\text{Fe}^{2+}_{(\text{aq})}$  at pH 6 - 8. The magnetite loading  
9  
10  
11 498 in all experiments was  $695 \text{ mg L}^{-1}$ .

pH	$[\text{Fe}^{2+}_{(\text{aq})}]_{\text{add}}$ ( $\mu\text{M}$ )	Ferrozine	lattice parameters	Micro-XRD	XMCD
		$\Delta[\text{Fe}^{2+}_{(\text{aq})}]^*$ ( $\mu\text{M}$ )	$\text{\AA}$	Fe(II)/Fe(III)	Fe(II)/Fe(III)
original	0	-	8.4050	0.544	0.538
6	0	575	8.3981	0.478	-
	1000	414	8.3984	0.481	-
	0	250	8.4003	0.498	0.604
7	500	150	-	-	0.754
	1000	19	8.4015	0.511	0.714
	0	0	8.4031	0.526	0.593
8	500	-425	-	-	0.634
	1000	-555	8.4043	0.538	0.610

27  
28 499 <sup>a</sup> Negative values in  $\Delta[\text{Fe}^{2+}_{(\text{aq})}]$  represent  $\text{Fe}^{2+}$  uptake to magnetite, and positive values  
29  
30 500 represent  $\text{Fe}^{2+}$  release from magnetite

31  
32 501  
33 502  
34  
35  
36  
37  
38  
39  
40  
41  
42  
43  
44  
45  
46  
47  
48  
49  
50  
51  
52  
53  
54  
55  
56  
57  
58  
59  
60

1  
2  
3  
4 503 Table 2. Changes of  $\text{Fe}^{2+}_{(\text{aq})}$  concentration based on chemical analysis and structurally ordered  
5  
6 504 Fe(II) in NPs measured by  $\mu\text{XRD}$ .

pH	$[\text{Fe}^{2+}_{(\text{aq})}]_{\text{added}}^{\text{a}}$ ( $\mu\text{M}$ )	$\Delta[\text{Fe}^{2+}_{(\text{aq})}]^{\text{b}}$ ( $\mu\text{M}$ )	$[\text{Fe(II)}_{\text{str}}]^{\text{c}}$ ( $\mu\text{M}$ )	$[\text{Fe(III)}_{\text{str}}]^{\text{d}}$ ( $\mu\text{M}$ )	$[\text{Fe}_{\text{tot}}]^{\text{e}}$ ( $\mu\text{M}$ )	$\Delta[\text{Fe(II)}_{\text{str}}]^{\text{f}}$ ( $\mu\text{M}$ )
original	0	0	3000	5516	8516	--
7	0	250	2748	5518	8266	-252
7	1000	19	2874	5623	8497	-126

15 505 <sup>a</sup> The concentration of  $\text{Fe}^{2+}_{(\text{aq})}$  that was initially added.

17 506 <sup>b</sup> The difference between equilibrium and initial concentrations of  $\text{Fe}^{2+}_{(\text{aq})}$

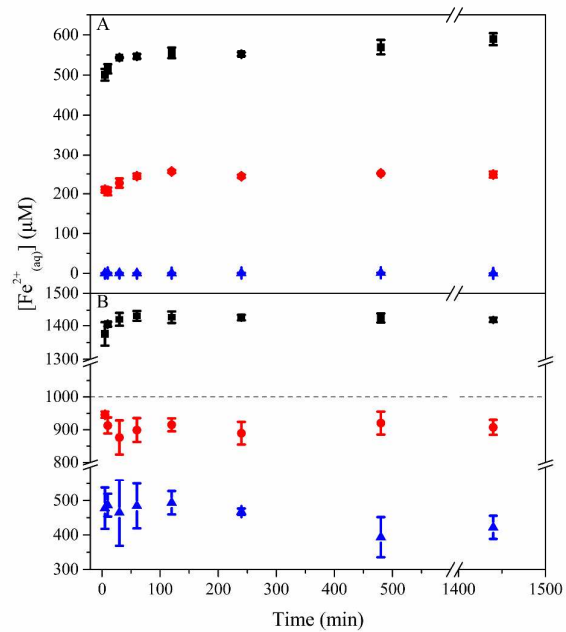
19 507 <sup>c</sup> The concentration of structural Fe(II) equivalent in magnetite NPs equilibrated with the pH 7  
21  
22 508 buffer solution, which was calculated from the  $\mu\text{XRD}$  results in Table 1.

23 509 <sup>d</sup> The concentration of structural Fe(III) equivalent in magnetite NPs equilibrated with the pH 7  
25  
26 510 buffer solution.

27 511 <sup>e</sup>  $[\text{Fe}_{\text{tot}}] = [\text{Fe(II)}_{\text{str}}] + [\text{Fe(III)}_{\text{str}}]$

28 512 <sup>f</sup> the change of structural Fe(II) concentration after equilibrated at pH 7 with or without added  
29  
30 513  $\text{Fe(II)}_{(\text{aq})}$

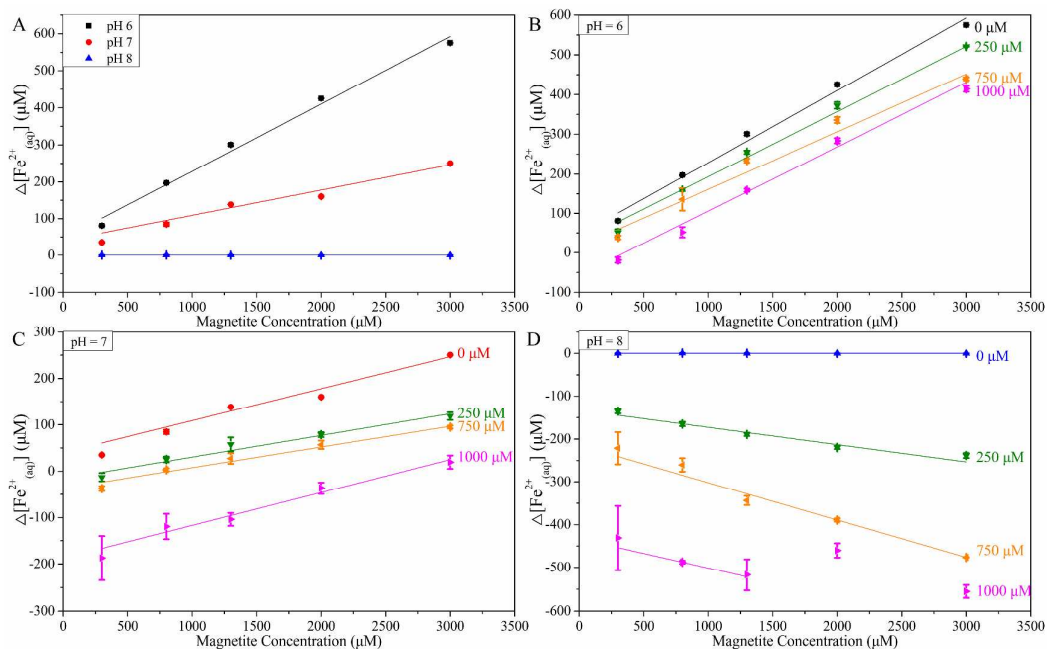
31  
32  
33  
34  
35  
36  
37  
38  
39  
40  
41  
42  
43  
44  
45  
46  
47  
48  
49  
50  
51  
52  
53  
54  
55  
56  
57  
58  
59  
60



514

515 **Figure 1.** Change of  $[\text{Fe}^{2+}_{(\text{aq})}]$  as a function of time in the suspensions of magnetite NPs ( $3000 \mu\text{M}$ 516 Fe(II) equivalent) at pH 6 (black), 7 (red), and 8 (blue), respectively, without amended  $\text{Fe}^{2+}_{(\text{aq})}$  (A)517 or in the presence of  $1000 \mu\text{M}$   $\text{Fe}^{2+}_{(\text{aq})}$  (B). The dashed line in (B) corresponds to  $[\text{Fe}^{2+}_{(\text{aq})}] = 1000$ 518  $\mu\text{M}$ .

519



520

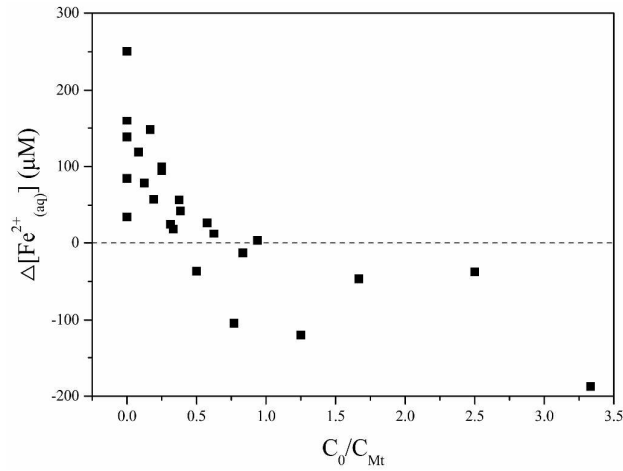
521 **Figure 2.** The change of  $\Delta[\text{Fe}^{2+}]_{\text{aq}}$  as a function of magnetite NPs loading without added  $\text{Fe}^{2+}_{\text{aq}}$

522 (A), and in the presence of 0  $\mu\text{M}$  (black), 250  $\mu\text{M}$  (green), 750  $\mu\text{M}$  (orange), or 1000  $\mu\text{M}$  (magenta)

523  $\text{Fe}^{2+}_{\text{aq}}$  at pH 6 (B), pH 7 (C), and pH 8 (D), respectively. The equation and  $R^2$  of the fitted lines

524 are shown in Table S2.

525

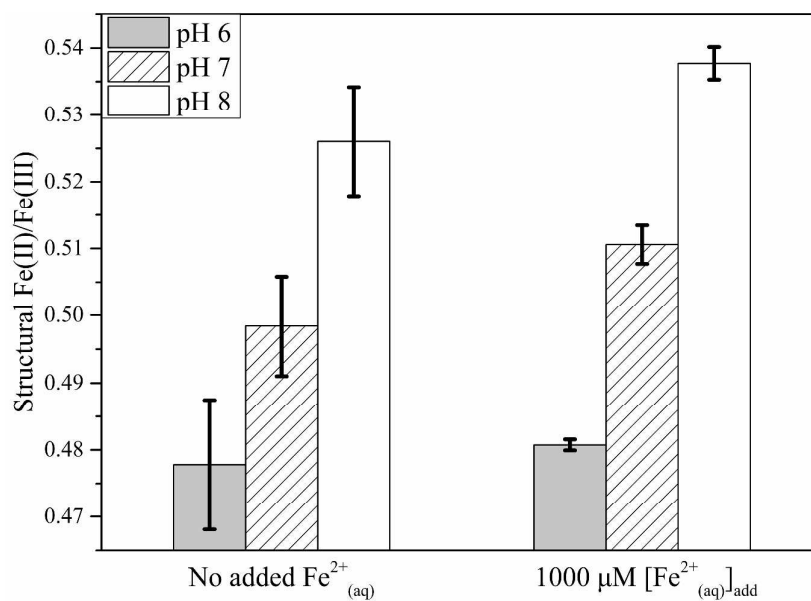


526

527 **Figure 3.**  $\Delta[\text{Fe}^{2+}_{(\text{aq})}]$  versus the ratio of initial  $[\text{Fe}^{2+}_{(\text{aq})}]$  ( $C_0$ ) to magnetite loading ( $C_{\text{Mt}}$ ) at pH 7.528 Positive values of  $\Delta[\text{Fe}^{2+}_{(\text{aq})}]$  indicate  $\text{Fe}^{2+}$  release from magnetite NPs, whereas negative values529 represent  $\text{Fe}^{2+}$  uptake by magnetite NPs.

530

531

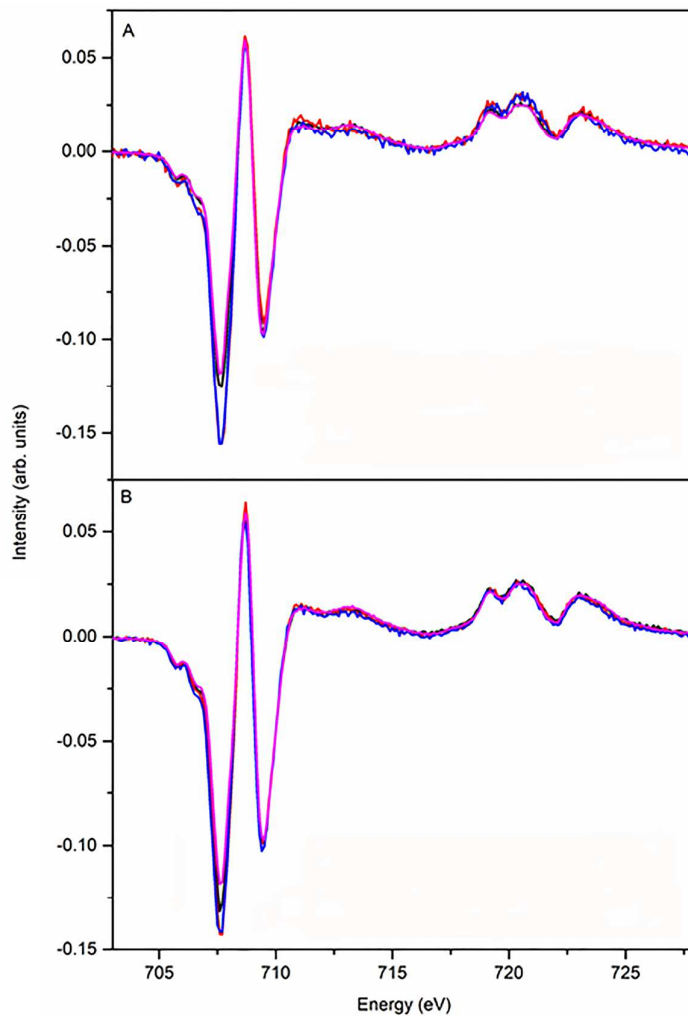


532

533 **Figure 4.** Structural Fe(II)/Fe(III) ratios of magnetite NPs ( $695 \text{ mg L}^{-1}$ ) without added  $\text{Fe}^{2+}_{(\text{aq})}$  (left)  
534 and in the presence of  $1000 \mu\text{M Fe}^{2+}_{(\text{aq})}$  (right), respectively, at pH 6, pH 7, and pH 8 from the  
535 measured lattice parameters by  $\mu\text{XRD}$ .

536

1  
2  
3  
4  
5  
6  
7  
8  
9  
10  
11  
12  
13  
14  
15  
16  
17  
18  
19  
20  
21  
22  
23  
24  
25  
26  
27  
28  
29  
30  
31  
32  
33  
34  
35  
36  
37  
38  
39  
40  
41  
42  
43  
44  
45  
46  
47  
48  
49  
50  
51  
52  
53  
54  
55  
56  
57  
58  
59  
60

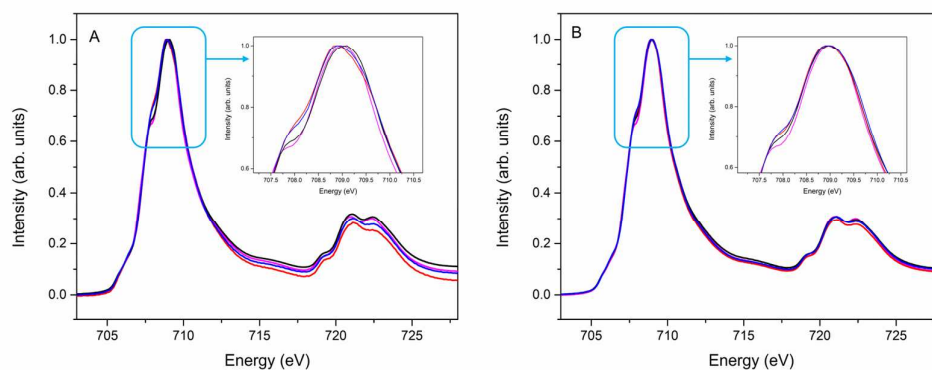


537

538 **Figure 5.** Comparison of XMCD spectra of magnetite NPs in stock suspension (magenta), in the539 buffer solution (black), and in the buffer solution with 500  $\mu\text{M}$  (red) or 1000  $\mu\text{M}$  (blue) added540  $\text{Fe}^{2+}_{(\text{aq})}$  at pH 7 (A) and 8 (B).

541





542

543 **Figure 6.** Comparison of XAS spectra of magnetite NPs in stock suspension (magenta), in the544 buffer solution (black), and in the buffer solution with 500  $\mu\text{M}$  (red) or 1000  $\mu\text{M}$  (blue) added545  $\text{Fe}^{2+}_{(\text{aq})}$  at pH 7 (A) and 8 (B).

546

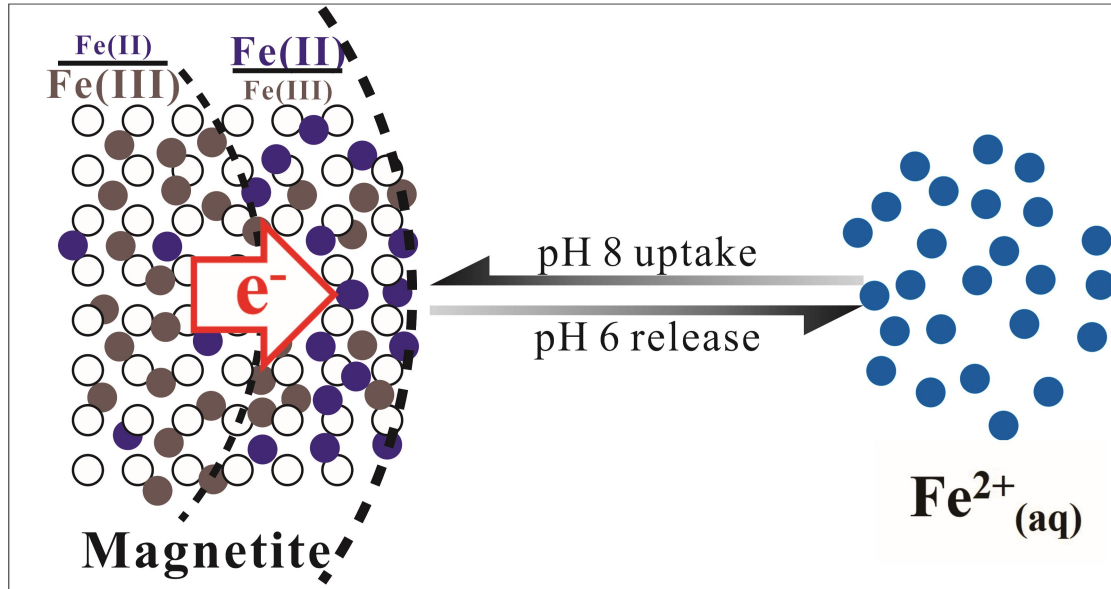
547 **Notes and references**

548

- 549 1. J. Liu, C. I. Pearce, O. Qafoku, E. Arenholz, S. M. Heald and K. M. Rosso, Tc(VII)  
550 reduction kinetics by titanomagnetite ( $\text{Fe}_{3-x}\text{Ti}_x\text{O}_4$ ) nanoparticles, *Geochim. Cosmochim.*  
551 *Acta*, 2012, **92**, 67-81.
- 552 2. C. I. Pearce, J. Liu, D. R. Baer, O. Qafoku, S. M. Heald, E. Arenholz, A. E. Grosz, J. P.  
553 McKinley, C. T. Resch, M. E. Bowden, M. H. Engelhard and K. M. Rosso,  
554 Characterization of natural titanomagnetites ( $\text{Fe}_{3-x}\text{Ti}_x\text{O}_4$ ) for studying heterogeneous  
555 electron transfer to Tc(VII) in the Hanford subsurface, *Geochim. Cosmochim. Acta*, 2014,  
556 **128**, 114-127.
- 557 3. C. A. Gorski and M. M. Scherer, Influence of magnetite stoichiometry on  $\text{Fe}^{\text{II}}$  uptake and  
558 nitrobenzene reduction, *Environ. Sci. Technol.*, 2009, **43**, 3675-3680.
- 559 4. J. Liu, C. I. Pearce, C. Liu, Z. Wang, L. Shi, E. Arenholz and K. M. Rosso,  $\text{Fe}_{3-x}\text{Ti}_x\text{O}_4$   
560 nanoparticles as tunable probes of microbial metal oxidation, *J. Am. Chem. Soc.*, 2013,  
561 **135**, 8896-8907.
- 562 5. R. M. Cornell and U. Schwertmann, *The Iron Oxides: Structure, Properties, Reactions,*  
563 *Occurrences and Uses*, Wiley-VCH, Weinheim, 2003.
- 564 6. D. C. Smith and B. McEnaney, The influence of dissolved oxygen concentration on the  
565 corrosion of grey cast iron in water at 50°C, *Corros. Sci.*, 1979, **19**, 379-394.
- 566 7. T. Ahn, J. H. Kim, H.-M. Yang, J. W. Lee and J.-D. Kim, Formation Pathways of  
567 Magnetite Nanoparticles by Coprecipitation Method, *J. Phys. Chem. C*, 2012, **116**,  
568 6069-6076.
- 569 8. P. Xu, G. M. Zeng, D. L. Huang, C. L. Feng, S. Hu, M. H. Zhao, C. Lai, Z. Wei, C.  
570 Huang, G. X. Xie and Z. F. Liu, Use of iron oxide nanomaterials in wastewater treatment:  
571 A review, *Sci. Total Environ.*, 2012, **424**, 1-10.
- 572 9. Q. A. Pankhurst, J. Connolly, S. K. Jones and J. Dobson, Applications of magnetic  
573 nanoparticles in biomedicine, *J. Phys. D: Appl. Phys.*, 2003, **36**, R167-R181.
- 574 10. V. Tishchenko, C. Meile, M. M. Scherer, T. S. Pasakarnis and A. Thompson,  $\text{Fe}^{2+}$   
575 catalyzed iron atom exchange and re-crystallization in a tropical soil, *Geochim.*  
576 *Cosmochim. Acta*, 2015, **148**, 191-202.
- 577 11. B. Zinder, G. Furrer and W. Stumm, The coordination chemistry of weathering: II.  
578 Dissolution of Fe(III) oxides, *Geochim. Cosmochim. Acta*, 1986, **50**, 1861-1869.
- 579 12. C. Colombo, G. Palumbo, J.-Z. He, R. Pinton and S. Cesco, Review on iron availability in  
580 soil: interaction of Fe minerals, plants, and microbes, *J. Soils Sediments*, 2014, **14**,  
581 538-548.
- 582 13. J. K. Fredrickson, J. M. Zachara, D. W. Kennedy, R. K. Kukkadapu, J. P. McKinley, S. M.  
583 Heald, C. Liu and A. E. Plymale, Reduction of  $\text{TcO}_4^-$  by sediment-associated biogenic  
584 Fe(II), *Geochim. Cosmochim. Acta*, 2004, **68**, 3171-3187.
- 585 14. J. Klausen, S. P. Troeber, S. B. Haderlein and R. P. Schwarzenbach, Reduction of  
586 substituted nitrobenzenes by Fe(II) in aqueous mineral suspensions, *Environ. Sci.*  
587 *Technol.*, 1995, **29**, 2396-2404.
- 588 15. C. A. Gorski and M. S. Fantle, Stable mineral recrystallization in low temperature  
589 aqueous systems: A critical review, *Geochim. Cosmochim. Acta*, 2017, **198**, 439-465.

- 1  
2  
3 590 16. R. Marsac, M. Pasturel and K. Hanna, Reduction kinetics of nitroaromatic compounds by  
4 591 titanium-substituted magnetite, *J. Phys. Chem. C*, 2017, **121**, 11399-11406.
- 5 592 17. D. E. Latta, C. A. Gorski, M. I. Boyanov, E. J. O'Loughlin, K. M. Kemner and M. M.  
6 593 Scherer, Influence of magnetite stoichiometry on U<sup>VI</sup> reduction, *Environ. Sci. Technol.*,  
7 594 2012, **46**, 778-786.
- 8 595 18. P. Dhakal, C. J. Matocha, F. E. Huggins and M. M. Vandiviere, Nitrite reactivity with  
9 596 magnetite, *Environ. Sci. Technol.*, 2013, **47**, 6206-6213.
- 10 597 19. C. A. Gorski, R. M. Handler, B. L. Beard, T. Pasakarnis, C. M. Johnson and M. M.  
11 598 Scherer, Fe atom exchange between aqueous Fe<sup>2+</sup> and magnetite, *Environ. Sci. Technol.*,  
12 599 2012, **46**, 12399-12407.
- 13 600 20. A. J. Friedrich, B. L. Beard, M. M. Scherer and C. M. Johnson, Determination of the  
14 601 Fe(II)aq-magnetite equilibrium iron isotope fractionation factor using the three-isotope  
15 602 method and a multi-direction approach to equilibrium, *Earth. Planet. Sci. Lett.*, 2014, **391**,  
16 603 77-86.
- 17 604 21. R. M. Handler, B. L. Beard, C. M. Johnson and M. M. Scherer, Atom exchange between  
18 605 aqueous Fe(II) and goethite: An Fe isotope tracer study, *Environ. Sci. Technol.*, 2009, **43**,  
19 606 1102-1107.
- 20 607 22. P. Larese-Casanova and M. M. Scherer, Fe(II) sorption on hematite: New insights based  
21 608 on spectroscopic measurements, *Environ. Sci. Technol.*, 2007, **41**, 471-477.
- 22 609 23. A. J. Friedrich, M. Helgeson, C. Liu, C. Wang, K. M. Rosso and M. M. Scherer, Iron  
23 610 Atom Exchange between Hematite and Aqueous Fe(II), *Environ. Sci. Technol.*, 2015, **49**,  
24 611 8479-8486.
- 25 612 24. P. Joshi and C. A. Gorski, Anisotropic Morphological Changes in Goethite during  
26 613 Fe<sup>2+</sup>-Catalyzed Recrystallization, *Environ. Sci. Technol.*, 2016, **50**, 7315-7324.
- 27 614 25. E. Silvester, L. Charlet, C. Tournassat, A. Géhin, J.-M. Grenèche and E. Liger, Redox  
28 615 potential measurements and Mössbauer spectrometry of Fe<sup>II</sup> adsorbed onto Fe<sup>III</sup>  
29 616 (oxyhydr)oxides, *Geochim. Cosmochim. Acta*, 2005, **69**, 4801-4815.
- 30 617 26. C. I. Pearce, O. Qafoku, J. Liu, E. Arenholz, S. M. Heald, R. K. Kukkadapu, C. A. Gorski,  
31 618 C. M. B. Henderson and K. M. Rosso, Synthesis and properties of titanomagnetite  
32 619 (Fe<sub>3-x</sub>Ti<sub>x</sub>O<sub>4</sub>) nanoparticles: A tunable solid-state Fe(II/III) redox system, *J. Colloid*  
33 620 *Interface Sci.*, 2012, **387**, 24-38.
- 34 621 27. C. A. Gorski and M. M. Scherer, Fe<sup>2+</sup> sorption at the Fe oxide-water interface: A revised  
35 622 conceptual framework, *Aq. Redox Chem.*, 2011, **1071**, 315-343.
- 36 623 28. C. I. Pearce, C. M. B. Henderson, N. D. Telling, R. A. D. Patrick, J. M. Charnock, V. S.  
37 624 Coker, E. Arenholz, F. Tuna and G. van der Laan, Fe site occupancy in  
38 625 magnetite-ulvöspinel solid solutions: A new approach using X-ray magnetic circular  
39 626 dichroism, *Am. Mineral.*, 2010, **95**, 425-439.
- 40 627 29. S. Gota, M. Gautier-Soyer and M. Sacchi, Fe 2p absorption in magnetic oxides:  
41 628 Quantifying angular-dependent saturation effects, *Phy. Rev. B*, 2000, **62**, 4187-4190.
- 42 629 30. R. A. D. Patrick, G. Van Der Laan, C. M. B. Henderson, P. Kuiper, E. Dudzik and D. J.  
43 630 Vaughan, Cation site occupancy in spinel ferrites studied by X-ray magnetic circular  
44 631 dichroism, *Eur. J. Mineral.*, 2002, **14**, 1095-1102.
- 45 632 31. A. F. White and M. L. Peterson, Reduction of aqueous transition metal species on the  
46 633 surfaces of Fe(II) -containing oxides, *Geochim. Cosmochim. Acta*, 1996, **60**, 3799-3814.

- 1  
2  
3 634 32. C. A. Gorski, R. Edwards, M. Sander, T. B. Hofstetter and S. M. Stewart,  
4 635 Thermodynamic characterization of iron oxide–aqueous Fe<sup>2+</sup> redox couples, *Environ. Sci.*  
5 636 *Technol.*, 2016, **50**, 8538-8547.  
6 637 33. E. Tronc, J. P. Jolivet, P. Belleville and J. Livage, Redox phenomena in spinel iron oxide  
7 638 colloids induced by adsorption, *Hyperfine Interact.*, 1989, **46**, 635-643.  
8 639 34. B. R. Coughlin and A. T. Stone, Nonreversible adsorption of divalent metal ions (Mn<sup>II</sup>,  
9 640 Co<sup>II</sup>, Ni<sup>II</sup>, Cu<sup>II</sup>, and Pb<sup>II</sup>) onto goethite: Effects of acidification, Fe<sup>II</sup> addition, and picolinic  
10 641 acid addition, *Environ. Sci. Technol.*, 1995, **29**, 2445-2455.  
11 642 35. P. J. Vikesland, R. L. Rebodos, J. Y. Bottero, J. Rose and A. Masion, Aggregation and  
12 643 sedimentation of magnetite nanoparticle clusters, *Environmental Science-Nano*, 2016, **3**,  
13 644 567-577.  
14 645 36. Y. You, S. Zheng, H. Zang, F. Liu, F. Liu and J. Liu, Stimulatory effect of magnetite on  
15 646 the syntrophic metabolism of Geobacter co-cultures: Influences of surface coating.,  
16 647 *Geochim. Cosmochim. Acta*, 2018, <https://doi.org/10.1016/j.gca.2018.1002.1009>.  
17 648 37. C. A. Gorski and M. M. Scherer, Determination of nanoparticulate magnetite  
18 649 stoichiometry by Mössbauer spectroscopy, acidic dissolution, and powder X-ray  
19 650 diffraction: A critical review, *Am. Mineral.*, 2010, **95**, 1017-1026.  
20 651 38. Y. Mamindy-Pajany, C. Hurel, N. Marmier and M. Roméo, Arsenic (V) adsorption from  
21 652 aqueous solution onto goethite, hematite, magnetite and zero-valent iron: Effects of pH,  
22 653 concentration and reversibility, *Desalination*, 2011, **281**, 93-99.  
23 654 39. J.-P. Jolivet and E. Tronc, Interfacial electron transfer in colloidal spinel iron oxide.  
24 655 Conversion of Fe<sub>3</sub>O<sub>4</sub>-γFe<sub>2</sub>O<sub>3</sub> in aqueous medium, *J. Colloid Interface Sci.*, 1988, **125**,  
25 656 688-701.  
26 657 40. S. V. Yanina and K. M. Rosso, Linked Reactivity at Mineral-Water Interfaces Through  
27 658 Bulk Crystal Conduction, *Science*, 2008, **320**, 218-222.  
28 659 41. J. G. Catalano, P. Fenter, C. Park, Z. Zhang and K. M. Rosso, Structure and oxidation  
29 660 state of hematite surfaces reacted with aqueous Fe(II) at acidic and neutral pH, *Geochim.*  
30 661 *Cosmochim. Acta*, 2010, **74**, 1498-1512.  
31 662 42. S. C. Pang, S. F. Chin and M. A. Anderson, Redox equilibria of iron oxides in  
32 663 aqueous-based magnetite dispersions: Effect of pH and redox potential, *J. Colloid*  
33 664 *Interface Sci.*, 2007, **311**, 94-101.  
34 665 43. J. M. Byrne, N. Klueglein, C. Pearce, K. M. Rosso, E. Appel and A. Kappler, Redox  
35 666 cycling of Fe(II) and Fe(III) in magnetite by Fe-metabolizing bacteria, *Science*, 2015, **347**,  
36 667 1473-1476.  
37  
38  
39  
40  
41  
42  
43  
44  
45 668  
46  
47  
48  
49  
50  
51  
52  
53  
54  
55  
56  
57  
58  
59  
60



The reversible flow of Fe(II) across the magnetite-solution interface impacts the stoichiometry and reactivity of magnetite nanoparticles.